Three-dimensional effects of an air curtain used to restrict cold room infiltration.

A.M. Foster[a]*, M.J. Swain[a], R. Barrett[b], P. D'Agaro [c], L.P. Ketteringham[a], S.J. James[a]

[a] *FRPERC, University of Bristol, Churchill Building, Langford, Bristol, BS40 5DU, UK, Tel: +44 (0)117 928 9239 Fax: +44 (0)117 928 9314*

[b] *Department of Aeronautical Engineering, University of Bristol, Queens Building, University Walk, Bristol, BS8 1TR, UK.*

c *Dipartimento di Energetica e Macchine, Universita degli Studi di Udine, via delle Scienze 208, I 33100 Udine, Italy*

*Corresponding author, E-mail: a.m.foster@bristol.ac.uk

Abstract

The aim of this study was to compare the measured effectiveness of an air curtain device at different jet velocities against a three-dimensional (3-D) computational fluid dynamics (CFD) model.   The air curtain device was not as wide as the entrance and had a geometry that encouraged 3-D flow.   By carefully setting up the air curtain an effectiveness of 0.71 was achieved compared to the initial value of only 0.31 as set by the air curtain device installer.   The 3-D CFD model predicted the infiltration through the entrance with no air curtain to an accuracy of within 20 to 32%. The predicted effectiveness, E, of the air curtain at different jet velocities was 0.10 to 0.15 lower than measured. The shape of the effectiveness curve against jet velocity was well predicted. CFD has shown that the flow from this air curtain cannot be considered as 2-D. The

1

central part of the jet is deflected away from the cold store by the Coanda effect caused by the air curtain device's fan body. The edges of the jet are deflected into the cold store by the stack pressures and turn into the void caused by the deflected central jet.

Notation

a_t	turbulent diffusivity, $m^2.s^{-1}$
b	thickness of air curtain jet, m
c_p	specific heat at constant pressure, $J.kg^{-1}.K^{-1}$
C	concentration of CO_2 in the room, %
C_μ	k-ε turbulence model constant, 0.09
$C_{\varepsilon 1}$	k-ε turbulence model constant, 1.44
$C_{\varepsilon 2}$	k-ε turbulence model constant, 1.92
D_m	deflection modulus, dimensionless
E	effectiveness, dimensionless
g	acceleration due to gravity, $9.81\ m.s^{-2}$
H	height of entrance, m
I	air exchange, dimensionless
k	turbulent kinetic energy per unit mass, $J.kg^{-1}$
Q	infiltration, m^3
p	static pressure, Pa
P	Shear production of turbulence, $kg.m^{-1}.s^{-3}$
t	time, s
$\overline{T}$	predicted average temperature, °C
ΔT	initial temperature difference between cold store and ambient, °C

3

u	air curtain jet velocity, $m.s^{-1}$
T	Temperature, K
w	velocity vector, $m.s^{-1}$
V	volume of air within the room, m^3

Greek

β	coefficient of thermal expansion, K^{-1}
δ	identity matrix, dimensionless
ε	turbulence dissipation rate, $m^2.s^{-3}$
λ	thermal conductivity, $W.m^{-1}.K^{-1}$
σ_ε	k-ε turbulence model constant, 1.3
σ_k	k-ε turbulence model constant, 1.0
σ_t	turbulent Prandtl number
μ	dynamic viscosity, $kg.m^{-1}s^{-1}$
ρ	density, $kg.m^{-3}$

Subscripts

a	with air curtain
b	without air curtain
o	supply air jet
ref	reference
t	turbulent

w   ambient

0   background

1   initial

2   final

Superscripts

—   turbulent mean quantities

'   turbulent fluctuating quantities

T   inverse matrix

1. Introduction

In 2002, the UK food and drinks industry used the equivalent of 285 thousand tonnes of oil to power its refrigeration [1] with most being used in cold stores. In cold stores energy is wasted due to air infiltration into the room during loading and unloading and other instances when the barrier between the cold and warm environments is removed. For an unprotected frozen storage room this exchange of air can cause the store to gain heat at the rate of approximately 105 kW per metre door width [2]. Air infiltration is also the main source of frost on evaporators and can lead to accidents caused by ice.

Transparent PVC strip curtains are the traditional and most commonly used method of reducing infiltration. Ligtenburg and Wijjfels [3] claim that 'they are generally considered as unsafe, not particularly efficient, unhygienic and requiring much maintenance and it is possible that they may be banned in the future.' Vestibules or air locks and flexible, fast-opening doors, often in combination with each other, are other methods employed to reduce infiltration. However, vestibules restrict access, are difficult to fit to existing sites and can be bulky, while flexible, fast-opening doors have heavy maintenance requirements and reduce vision for forklift truck operators.

Air curtains reduce infiltration without taking up as much space as vestibules and without impeding traffic. Their origin dates back to a patent applied for by Van Kennel in 1904 [4,5] and they have been popular for around 50 years. An air curtain consists of a fan unit that produces a planar jet of air (air curtain), which forms a barrier to heat, moisture, dust, odours, insects etc. In the case of cold store air curtains, the device that produces it is usually mounted above the door, blowing the air curtain vertically down. Some air curtains recirculate via a return duct opposite the air jet outlet, but most do not.

Measured values of the static effectiveness of air curtains as found installed on cold stores (before improvements were made) have been between 0.44 and 0.78 [6]. An effectiveness of 1 means that infiltration is totally eliminated, 0 means that there is no effect on the infiltration and a negative value indicates that the infiltration is worse than with no air curtain.

The basic theory for natural convection of fluids at different densities through openings was expressed more than 70 years ago [7]. Since then many authors have created improved models [8-13]. Most air curtains are essentially plane, turbulent jets and the physics of these jets are also well documented [14-16].

Solving the equations for natural convection through openings and also for turbulent jets allows the interaction between the air curtain and air infiltration through the entrance to be evaluated. Hayes and Stoecker [4,5] created analytical equations to predict heating and cooling loads across non-recirculatory air curtains. This theory deviated from measurements by about 15% for air curtain height to air jet thickness ratios of up to 84. Guyonnaud et al [17] demonstrated differences between the Hayes and Stoecker, and Lajos and Preszler [18] model. They showed that knowing the height of the air curtain, jet thickness and jet velocity was not sufficient to simply describe the fluid mechanics of the air curtain. The convection of jet vortices (large eddies) and the height of the impinging (or recompression) zone all affect the effectiveness of the air curtain sealing.

Ge and Tassou [19] used finite difference models with good success to predict the performance of air curtains for vertical refrigerated display cabinets. Due to the large computing power required by the finite difference models, the authors then based simplified correlation models on the predictions. Foster et al [20,21] investigated the

use of computational fluid dynamics (CFD) to predict flow through an unprotected cold store entrance and showed that it was generally qualitatively accurate.

A literature search found only one publication [3] where finite difference models have been used to predict the effectiveness of an air curtain for a cold store entrance, however this was a two dimensional (2-D) simulation and therefore did not take into account end effects. A three dimensional (3-D) finite difference model was used to investigate the design of an air curtain on a heated store; this study showed the importance of having an air curtain that extended beyond the width of the door [22]. No publications were found which describe the 3-D interactions between an air curtain and cold store. Only one publication was found that shows the relationship of real air curtain effectiveness with varying jet velocity [23].

The aim of this study was to compare the measured effectiveness of a commercially available air curtain at different jet velocities against a 3-D CFD model. The air curtain device used in the study had an outlet that was not as wide as the entrance and had a geometry that encouraged three-dimensional flow. In this paper, 3-D flows predicted using CFD are compared to idealised, 2-D, planar flow predictions, which are often assumed. The accuracy of this model was compared to the analytical model presented by Hayes and Stoecker [5].

2. Materials and methods

2.1 Test room and air curtain

Experimental studies were carried out on a cold storage room (internal dimensions L x W x H = 4.8 m x 5.8 m x 3.8 m), which was used in previous studies by Foster et al [20,21]. This cold storage room was inside a food-processing hall of floor dimensions

24 m x 17 m. The room had an entrance (W x H = 1.36 m x 3.2 m) with a 0.16 m
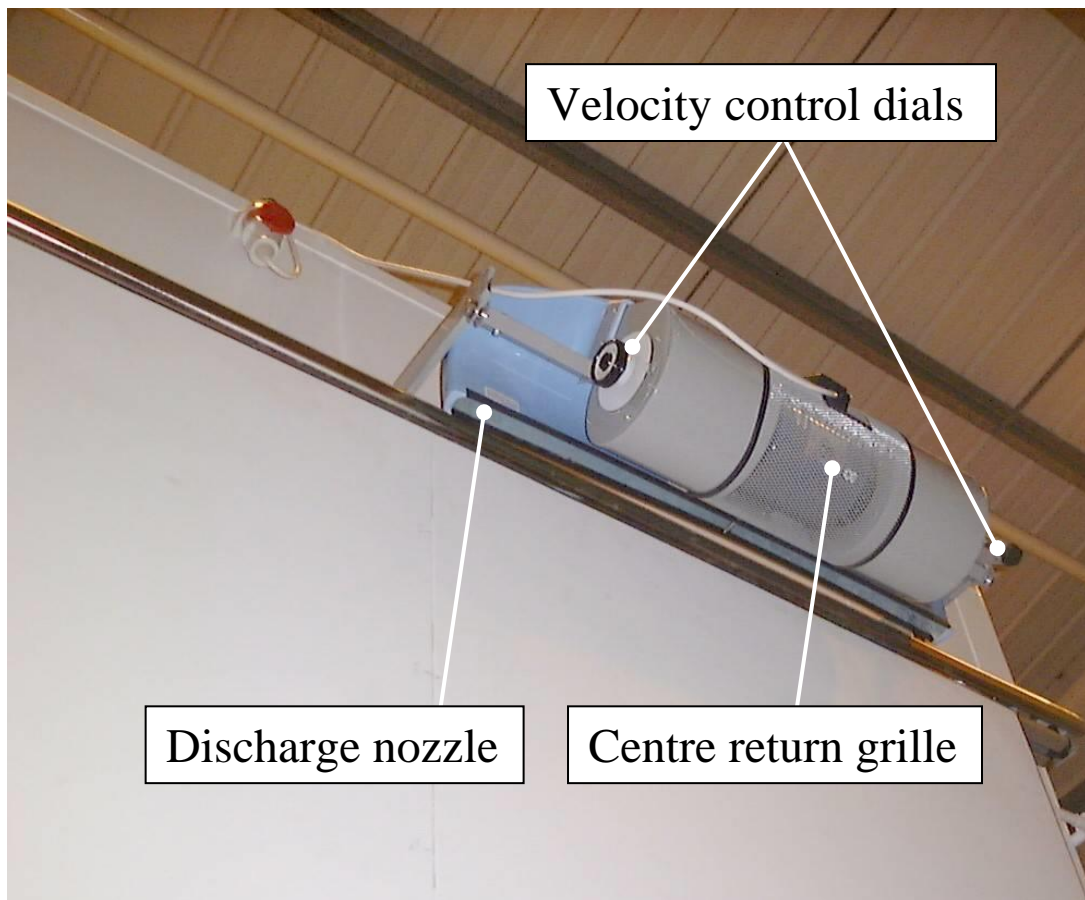
doorframe and was fitted with a sliding door.

Figure 1 The air curtain device as viewed from below after installation

An air curtain device (Model TS-40, Thermoscreens Ltd, UK) was fitted centrally above

the door on the outside of the cold store (Figure 1). The outlet of the air curtain device's

nozzle was positioned 160 mm from the outside surface of the cold store panels; the

door rail prevented closer fitting than this. The air curtain had a fan/blower housed in a

0.62 mm long cylindrical body. Air was drawn into the fan through a grille in the centre

of the cylindrical body. Air could also be drawn into each end of the cylindrical body,

through slide ports attached to a velocity control dial, allowing the velocity of the air

curtain to be increased. Air was blown out of the cylindrical body and through a duct

that turned the air through approximately 135° and discharged it through a nozzle with

dimensions of 1.0 m wide by 30 mm deep. The air curtain was fitted and set up by a contractor and was provided with controls to allow rotation of the air curtain device to provide different air curtain jet angles.

In later trials to compare results with an air curtain that covered the full width of the door, the entrance was reduced to 1.0 m wide so that the air curtain width matched the door width without overlaps.

2.2 Measurements

Measurements of the jet velocity were made across the width of the air curtain, close to the outlet of the duct using a hot wire anemometer (Model 1650, Thermo Systems Inc, UK) (accuracy ±2%) whilst the door was fully open. Turbulence levels were not measured as Guyonnaud et al [17] showed that an initial turbulence intensity in the range of 0 to 20% had no effect on the air curtain performance and that commercial air curtains were in the range of 10 to 20% turbulence intensity. A range of turbulence intensities was modelled to verify this statement.

Air exchange was calculated by the measured decay of an elevated CO_2 concentration in the room over time. CO_2 was released into the room and mixed using the evaporator fans to give a concentration of approximately 0.5% (5 000 ppm). The concentration could not exceed 5 000 ppm due to safety implications. All CO_2 concentrations were measured to an accuracy of 250 ppm with an infra-red CO_2 analyser (Model ABPA-210, Horiba Ltd, Japan).

Immediately prior to each door-opening test, the evaporator fans were switched off to allow the air movement to settle for 30 s. The door was fully opened for 10 or 30 s and then closed. The door took a total of 6±1 s to open and the same to close. All trials

10

were carried out with an initial room temperature of -20°C. The air temperature outside the room was between 20 and 26°C.

It was assumed that the decay of CO_2 was logarithmic during the door opening and that the CO_2 fully mixed on entering the room. Concentrations measured immediately before and after the door-opening were used to calculate the infiltration as shown in Equation 1 [23].

$$Q = V.\ln\left(\frac{C_2 - C_0}{C_1 - C_0}\right) \qquad (1)$$

A door switch was fitted to start the air curtain device as the door started to open and stop it just after the door closed. Experiments were carried out for different air curtain velocities, ranging from the minimum (10.5 ms^{-1}) to the maximum (18 ms^{-1}) attainable velocities and with the air curtain switched off. A vertical jet angle was used for the variable jet velocity measurements.

The effectiveness (E) of the air curtain was derived from the measurements taken, at each condition, defined in Equation 2.

$$E = \frac{Q_b - Q_a}{Q_b} \qquad (2)$$

2.3 Analytical model

Hayes and Stoecker [5] have presented an analytical model to assist in the design of air curtains (Equation 3). Their model allows the calculation of the 'deflection modulus', which is the ratio of air curtain momentum to transverse forces, caused by temperature difference either side of the curtain (stack effect). The stack effect is created by the

difference in air densities on the two sides of the doorway and results in a linear variation in pressure from the top to the bottom of the opening.

$$D_m = \frac{b.u^2}{g.H^2.\left(\dfrac{T_o}{T_c} - \dfrac{T_o}{T_w}\right)} = \frac{\rho_o b.u^2}{g.H^2.(\rho_c - \rho_w)} \tag{3}$$

They also presented a chart showing the minimum outlet momentum required to maintain an unbroken curtain (Figure 2).
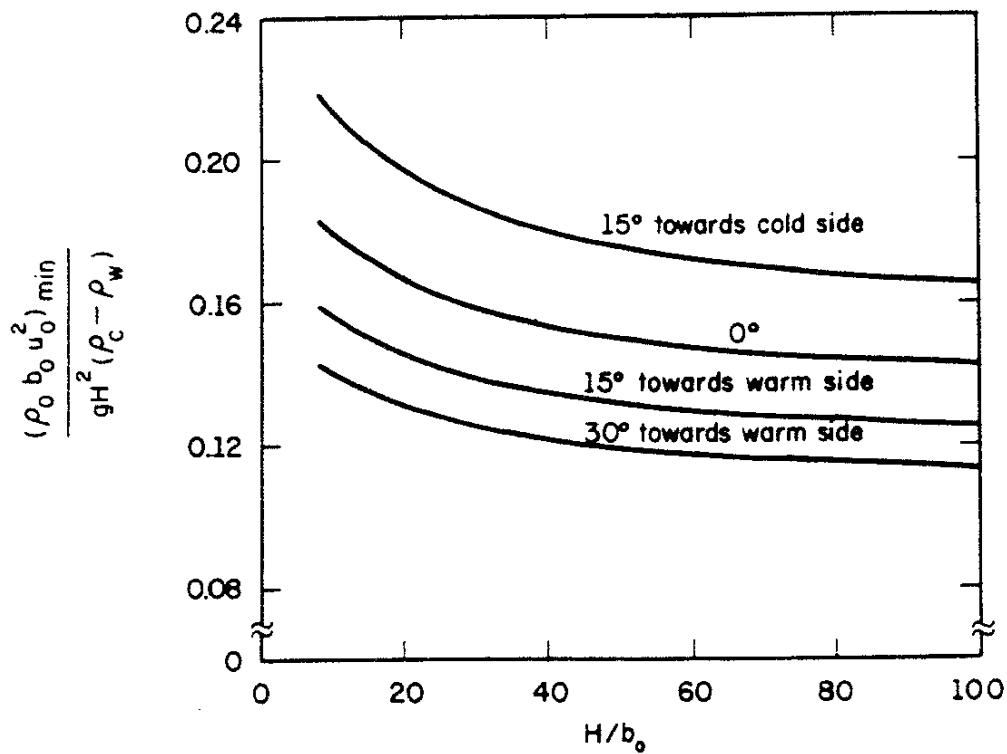

Figure 2. Minimum outlet momentum required to maintain an unbroken curtain.

From the chart and equation it is possible to calculate the minimum curtain velocity to provide an unbroken curtain. However, because this is the velocity at the borderline of stability, a higher outlet velocity must be selected in order to provide a factor of safety. They showed that heat transfer through the curtain is proportional to jet velocity for velocities above the borderline of stability and it is not therefore beneficial to have too

high a safety factor. The literature suggests a range of safety factors between 1.3 and

2.0 to use in this model [5], these were applied in this paper.

2.4 CFD model

A 3-D model was created using CFX 5.7.1 (ANSYS Inc., USA), a general purpose CFD

code. The hardware used to run the model was a Viglen Genie PC with an Intel

Pentium 4 processor running at 1.6 GHz with 1.25 Gb RAM.

2.4.1 Governing equations

The governing equations are written following the RANS (Reynolds Averaged Navier

Stokes) approach. Thus the instantaneous value of each variable ϕ is given by the sum of

its time averaged mean value $\bar{\phi}$ and a turbulent fluctuating component ϕ'.

The time-averaged continuity, momentum and energy equations for a constant property

incompressible fluid in absence of volumetric heating and neglecting the effects of

viscous dissipation can be written as follows in their conservative form:

$$\nabla \cdot \overline{\mathbf{w}} = 0 \tag{4}$$

$$\rho \, \frac{\partial \overline{\mathbf{w}}}{\partial t} + \rho \, \nabla \cdot \left(\overline{\mathbf{w}} \, \overline{\mathbf{w}} \right) = -\nabla \overline{p} + \mu \nabla^2 \overline{\mathbf{w}} + \rho \beta \left(\overline{T} - T_{ref} \right) \mathbf{g} - \nabla \cdot \left(\rho \, \overline{\mathbf{w}' \mathbf{w}'} \right) \tag{5}$$

$$\rho \, c_p \, \frac{\partial \overline{T}}{\partial t} + \rho \, c_p \nabla \cdot \left(\overline{\mathbf{w}} \, \overline{T} \right) = \lambda \, \nabla^2 \overline{T} - \nabla \cdot \left(\rho \, \overline{\mathbf{w}' T'} \right) \tag{6}$$

In the right hand side of equation 5 and 6 appear the unknown Reynolds stresses

$\left(\rho \overline{\mathbf{w}' \, \mathbf{w}'} \right)$ and Reynolds fluxes $\left(\rho \overline{\mathbf{w}' T'} \right)$ respectively.

As the temperature variations are in a range of values which allows the use of the

Boussinesq approximation to simulate buoyancy. Following such an approximation, the

density is assumed constant in the transient and convective terms, while it is linearly

dependent on temperature in the buoyancy term $\rho\beta(\overline{T} - T_{ref})\mathbf{g}$.

The k-ε turbulence model was adopted to model the Reynolds stresses and fluxes. As it

uses an eddy-viscosity hypothesis, the Reynolds stresses can be linearly related to the

mean velocity gradients as follows:

$$-\left(\rho\overline{\mathbf{w}'\,\mathbf{w}'}\right) = -\frac{2}{3}\rho k\delta - \frac{2}{3}\mu_t\nabla\cdot\overline{\mathbf{w}}\,\delta + \mu_t\left(\nabla\overline{\mathbf{w}} + \left(\nabla\overline{\mathbf{w}}\right)^T\right) \tag{7}$$

where μ_t is the turbulent viscosity, $k = 1/2\,\overline{(\mathbf{w}')^2}$ is the turbulent kinetic energy and δ is

the identity matrix. Analogously the Reynolds fluxes are linearly related to the mean

temperature gradient as

$$-\left(\rho\overline{\mathbf{w}'T'}\right) = -\rho\,c_p a_t\nabla\overline{T} \tag{8}$$

with

$$a_t = \frac{\mu_t}{\rho\sigma_t} \tag{9}$$

where a_t e σ_t are known as turbulent diffusivity and turbulent Prandtl number

respectively.

From this point on we drop the over bar on the mean quantities for the sake of

simplicity.

In the k-ε model, it is assumed that the turbulence viscosity is linked to the turbulence

kinetic energy and dissipation via equation 10.

$$\mu_t = C_\mu\rho\frac{k^2}{\varepsilon} \tag{10}$$

Where C_μ is a constant. The values of k and ε come directly from the differential transport equations for the turbulence kinetic energy and turbulence dissipation rate (equations 11 and 12).

$$\frac{\partial \rho k}{\partial t} + \nabla \cdot (\rho \mathbf{w} k) - \nabla \cdot \left[\left(\mu + \frac{\mu_t}{\sigma_k} \right) \nabla k \right] = P - \rho \varepsilon \qquad (11)$$

$$\frac{\partial \rho \varepsilon}{\partial t} + \nabla \cdot (\rho \mathbf{w} \varepsilon) - \nabla \cdot \left[\left(\mu + \frac{\mu_t}{\sigma_\varepsilon} \right) \nabla \varepsilon \right] = \frac{\varepsilon}{k} \left(C_{\varepsilon 1} P - C_{\varepsilon 2} \rho \varepsilon \right) \qquad (12)$$

where P is the shear production defined by:

$$P = \mu_t \nabla \mathbf{w} \cdot \left(\nabla \mathbf{w} + \nabla \mathbf{w}^{\mathrm{T}} \right) - \frac{2}{3} \nabla \cdot \mathbf{w} \left(\mu_t \nabla \cdot \mathbf{w} + \rho k \right) \qquad (13)$$

$C_{\varepsilon 1}$, $C_{\varepsilon 2}$, σ_k and σ_ε are constants.

To compare results with another turbulence model, the SSG Reynolds stress model [24] was also used at one condition. The Reynolds stress model does not use the eddy viscosity hypothesis, but solves equations for the transport of Reynolds stresses $\left(\rho \overline{\mathbf{w}' \mathbf{w}'} \right)$ in the fluid.

2.4.2 Boundary conditions

The air jet was an inlet type boundary condition with a constant velocity, temperature and turbulence intensity across it. The magnitude of the inlet velocity was varied from 10 to 26 m.s^{-1} and the direction was taken to be normal to the boundary. The temperature was fixed at 22°C and the turbulence intensity was 10% except for one case at 5 and 20%.

The return grille was modelled as an outlet with a relative static pressure. In this way the exit boundary condition pressure profile can float, but the average value was constrained to a specified value.

All boundaries except the inlet and outlet of the air curtain were modelled as no slip walls where the velocity of the fluid at the wall boundary was set to zero. Initially, an 'opening'-type boundary condition was used at the outer boundaries of the volume outside the cold store. This type of boundary condition allows simultaneous inflow and outflow and is useful if it is not known whether the flow will be entering or leaving through the boundary. This was found to generate numerically instabilities, so the outer boundaries of the volume outside the cold store were modelled as no slip walls and were placed far enough from the entrance so as not to influence the air curtain.

The wall-function approach is an extension of the method of Launder and Spalding [25]. In the log-law region, the near wall tangential velocity is related to the wall-shear-stress by means of a logarithmic relation. In the wall-function approach, the viscosity affected sublayer region is bridged by employing empirical formulas to provide near-wall boundary conditions for the mean flow and turbulence transport equations. These formulas connect the wall conditions (e.g., the wall-shear-stress) to the dependent variables at the near-wall mesh node which is presumed to lie in the fully-turbulent region of the boundary layer.

2.4.3 Initial conditions

The initial conditions of temperature of the cold store and outside were −20°C and +22°C respectively. The initial conditions of velocity throughout the domain were 0.

2.4.4 Discretisation

Equations 4-6 and 11-12 were solved using a finite volume technique. The advection scheme used was the High Resolution Scheme. This scheme varies the blend factor throughout the domain based on the local solution field in order to enforce a boundedness criterion. A blend factor of 0.0 is equivalent to using the First Order Advection Scheme and is the most robust option. A value of 1.0 uses Second Order differencing for the advection terms. In flow regions with low variable gradients, the Blend Factor will be close to 1.0 for accuracy. In areas where the gradients change sharply, the Blend Factor will be closer to 0.0 to prevent overshoots and undershoots and maintain robustness.

The transient scheme defines the discretisation algorithm for the transient term. The Second Order Backward Euler scheme was used. This is an implicit time-stepping scheme, and is second order accurate.

2.4.5 Geometry of the model

The domain of the model covered the cold store and a volume outside, in front of the cold store door (Figure 3). The modelled volume outside the cold store did not cover the full volume of the processing hall, as this would have required greater computer resources than were available.
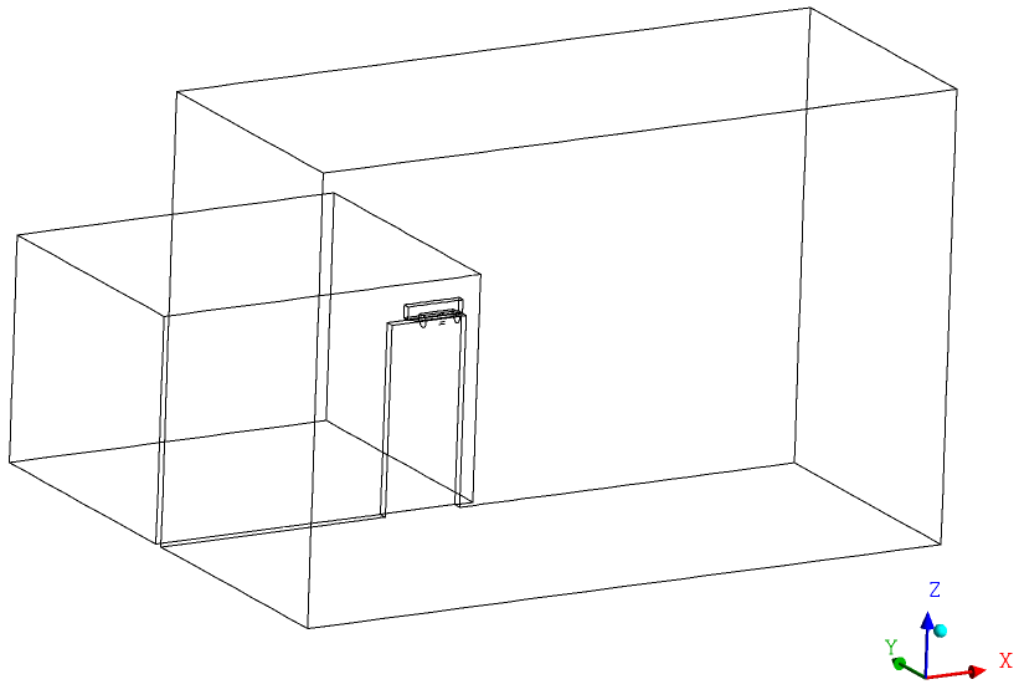
Figure 3: Isometric view of the modelled volumes, illustrating the position of the air curtain and entrance

The geometry of the modelled air curtain was an approximation of the real air curtain; the exact geometry would have required a finer mesh than was possible with the given computing resources when in conjunction with such a large domain (Figure 4). Important geometrical dimensions, such as the nozzle thickness and its relative position to the fan body were modelled as accurately as possible. The air return grille on the air curtain was modelled as being at the top of the air curtain. This was because the real return grille characteristics were complex and attempts at modelling it with the size of mesh used in the model caused un-realistic flows. The door rail obstructed entrainment to the room side of the outlet nozzle and so a simplified geometry was created to give the same effect (shown as the block labelled "simplified door rail" to the left of the outlet and return ducts in Figure 4).
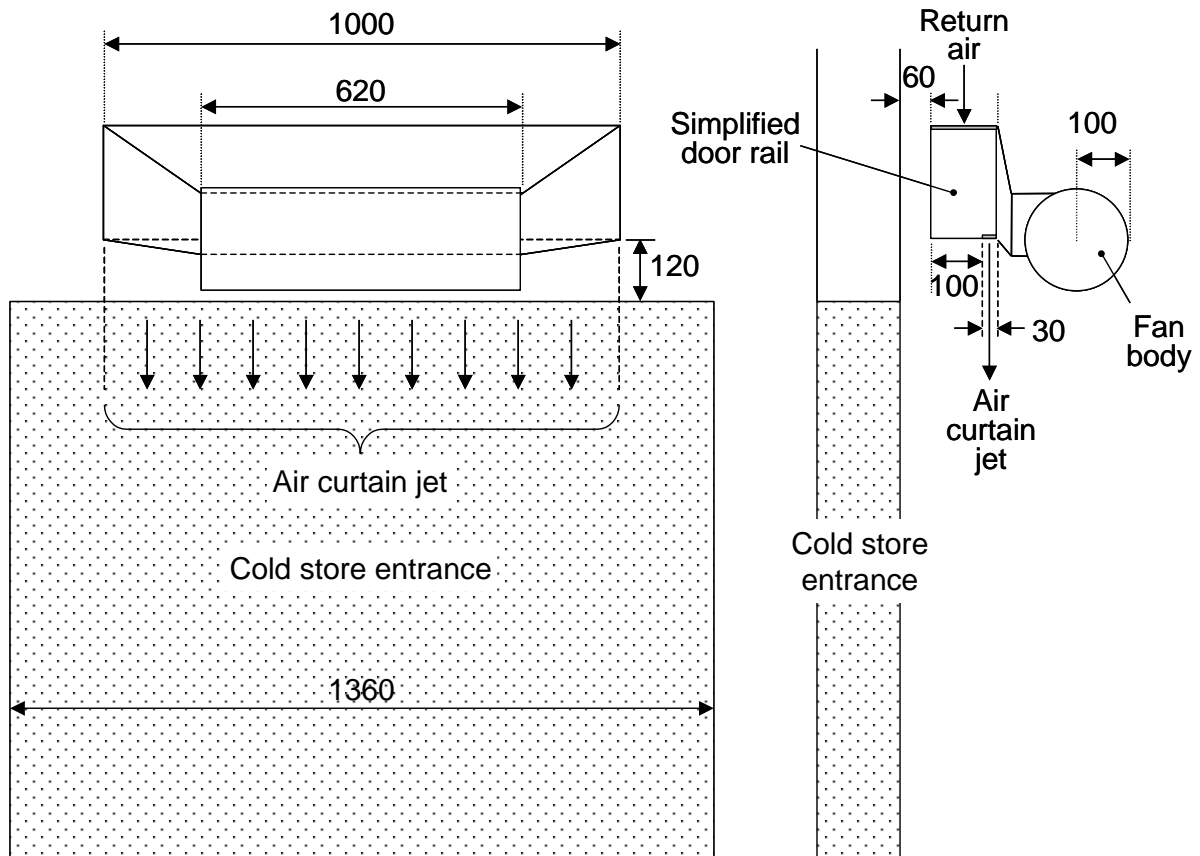
Figure 4: Front and side elevations of the modelled air curtain device and air curtain inlet and outlet boundaries. Dimensions in mm

The geometry was discretised with a tetrahedral mesh. The numerical mesh ranged from 30 mm at its finest point to 500 mm at its largest point, with an expansion factor of 1.2 between these mesh sizes. The width of the air jet boundary is the same as the minimum cell size, thus there is only one cell across the width of the air jet.

In the plane of the door entrance, and for a radius of 0.5 m from this plane, the mesh was 100 mm with an expansion factor of 1.2 outside the radius of influence. The total number of grid nodes for the model was 383 945. To test the convergence of the mesh, finer meshes were used on a 'cut down' geometry. This 'cut down' geometry was essentially the same, except a symmetry plane was used to reduce the number of mesh points. Mesh sizes of 100, 70 and 40 mm in the plane of the door entrance were

produced. Computer resources did not allow meshes smaller than 40 mm within the entrance in this model.

Computer simulation times were approximately 22 hours for a transient run of 30 s with a mesh size of 100 mm to a normalised residual of 1 x 10^{-4}. For each solution variable, φ, the normalised residual r'_ϕ is given in general by equation 14.

$$[r'_\phi] = \frac{[r_\phi]}{a_p \Delta \phi}$$

(14)

where r_ϕ is the raw residual control volume imbalance, a_p is representative of the control volume coefficient and $\Delta \phi$ is a representative range of the variable in the domain.

2.4.6 Predictions of air exchange

The CFD model was used to predict the air exchange between the cold store and the surroundings and the effectiveness of the air curtain at differing jet velocities. Infiltration was calculated for door-open durations of 10 and 30 s from the predicted average temperature inside the cold store. The change in mean cold store temperature (T_2) follows the same logarithmic relationship as that in Equation 1, as shown in Equation 15.

$$Q = V.\ln\left(\frac{T_w - T_2}{T_w - T_1}\right)$$

(15)

To represent the air exchange in a more universal manner, a dimensionless air exchange parameter, I, is defined in Equation 16. An air exchange of 1.0 corresponds to the whole volume of the cold store exchanging with the outside.

20

$$I = \frac{Q}{V} \tag{16}$$

Significant distortion of the air curtain from its ideal planar shape was thought to be due to the Coanda effect. This was especially true in the area where the air curtain flowed out of the nozzle, close to the cylindrical fan body. This shape would be likely to cause bending of the air curtain towards the fan body due to its proximity, but was less wide than the air curtain and so would cause more distortion in the centre of the curtain than the outer parts.
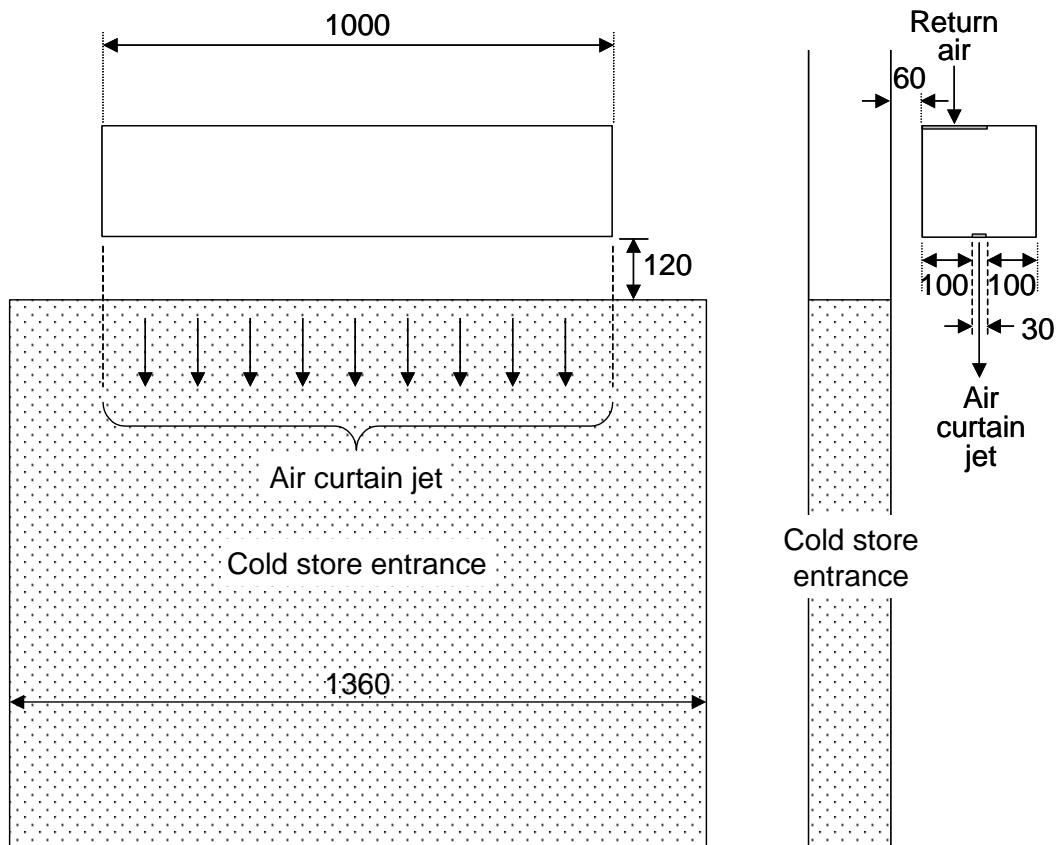

Figure 5: Front and side elevations of the simplified, symmetrical modelled air curtain device and air curtain inlet and outlet boundaries

To evaluate the effect of this asymmetry on the jet flow, a simplified air curtain was also modelled. This was created such that the combination of the simplified door rail, which was the same shape as used in the original model, and the device's body made a shape

that was symmetrical either side of the air curtain plane (Figure 5). The symmetrical curtain had the same inlet and outlet positions as the previous model.

3. Results and discussion

3.1 Initial measurements

Infiltration without the air curtain operating was measured as 14.9 (standard deviation of 1.0) and 51.2 (standard deviation of 0.4) m^3 for a door-open time of 10 and 30 s respectively. This gave an air exchange of 0.14 and 0.49 for a door-open time of 10 and 30 s respectively.

Trials were carried out on the air curtain as commissioned by the contractor, who set it to its lowest velocity and pointing vertically downwards. The jet velocity of the air curtain across the width of the duct averaged 10.5 $m.s^{-1}$. The measured effectiveness of the air curtain was 0.2 for a door-open duration of 10 s and 0.31 for 30 s.

3.2 Optimisation

Figure 6 shows the effectiveness of the air curtain for a door-open duration of 30 s and for different air jet velocities at an angle of 0° to the vertical. The effectiveness of the air curtain was increased from a minimum of 0.31 with a jet velocity of 10.5 $m.s^{-1}$ (as installed) to a maximum of 0.71 with a jet velocity of 18 $m.s^{-1}$, which was the highest jet velocity obtainable.
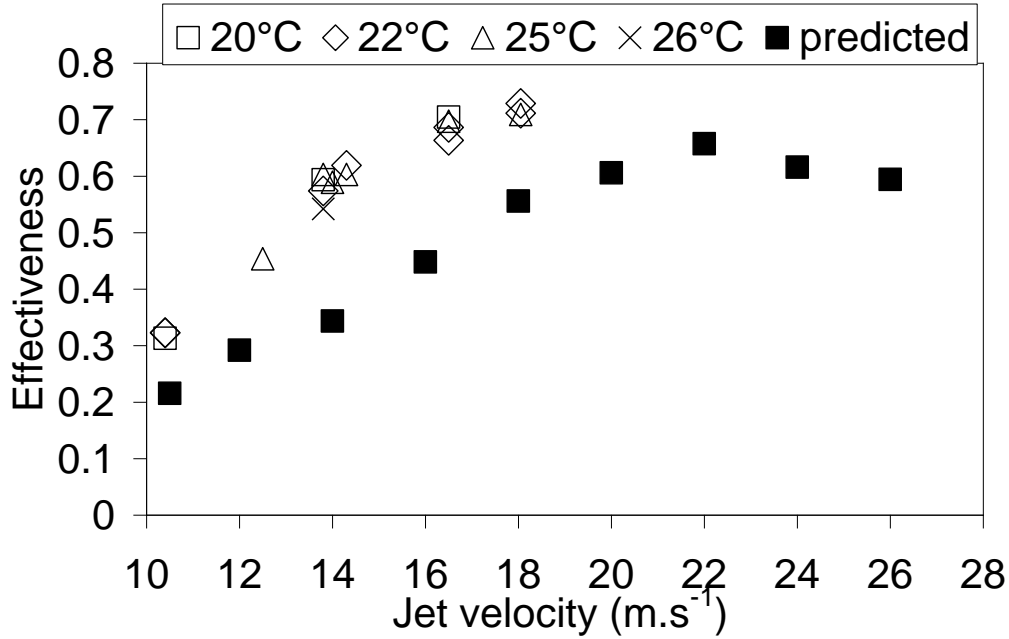
Figure 6. Measured and predicted effectiveness of the air curtain for different air jet velocities for a door-open duration of 30s and jet angle of 0°. The measurements were taken at different outside temperatures (shown in the legend).

3.3 Analytical predictions

From equation 3 the deflection modulus was calculated as 0.24 for the air curtain with a jet velocity of 10.5 m.s^{-1}. By slight extrapolation of the curve in figure 2, for an angle of 0°, it was calculated that the minimum discharge momentum for this air curtain, which had a door height to jet thickness ratio of 107, is approximately 0.15.

To calculate the minimum velocity required to achieve a continuous air curtain across the entrance given a known deflection modulus, equation 3 can be re-arranged to give equation 17.

$$u_m = \sqrt{D_m \cdot g \cdot \frac{H^2}{b} \cdot \left(\frac{T_o}{T_c} - \frac{T_o}{T_w} \right)} \tag{17}$$

Applying equation 17, a minimum velocity of 8.3 m.s^{-1} was calculated. This is the minimum recommended velocity; in practice a safety factor of between 1.3 and 2.0 is

commonly used. Using this range of safety factors, a number of velocities can be chosen from 11 to 17 m.s^{-1}. Using these velocities in figure 6 results in an effectiveness of the air curtain varying from 0.37 to 0.70. A higher safety factor of 2.2 yields the best effectiveness in these tests. This range of velocities shows that the jet should have been powerful enough to reach the floor at all available velocities, though the minimum velocity of 10.5 m.s^{-1} is just below the velocity calculated with a minimum safety factor of 1.3.

3.4 CFD predictions

Air exchange without the air curtain device operating was predicted as 0.19 and 0.58 for a door-open time of 10 and 30 s respectively. This was 32% and 20% higher than measured for the door-open times of 10 and 30 s respectively.

Figure 6 shows that the predicted effectiveness was always lower than measured (0.10 lower at the minimum and 0.15 lower at the maximum measured velocity). The trends of the predicted and measured data are similar up to the maximum measured velocity, in that they have a similar, positive gradient that reduces with jet velocity. The predicted effectiveness reaches a maximum of 0.66 at a jet velocity of 22 m.s^{-1}. It was not possible to increase the measured jet velocity above 18 m.s^{-1} in these experiments due to limitations in the installed system, however, the only data found in the literature [23] shows the shape of the predicted curve to be accurate, essentially a polynomial curve with one maximum effectiveness at a specific velocity. It is not possible to predict at what jet velocity the maximum effectiveness would be from the data. However, the (average) positive gradient between the highest two measured velocities indicates that the maximum effectiveness would be greater than 0.72, at a jet velocity above 18 m.s^{-1}.
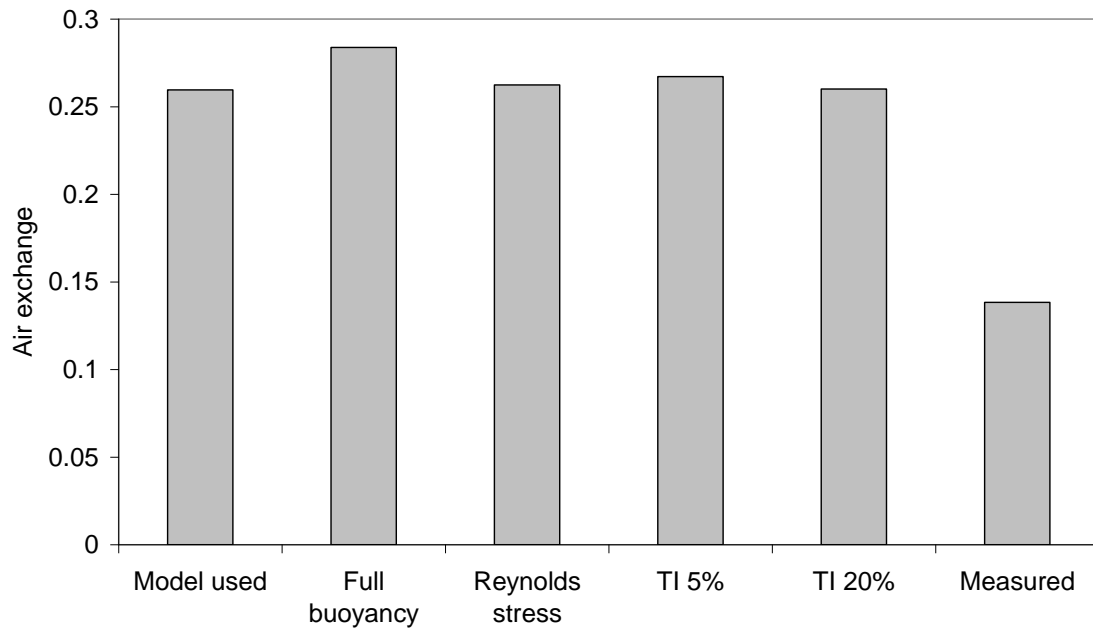
Figure 7. Predicted air exchange at a jet velocity of 18 m.s^{-1} for a door open duration of 30 s with different model assumptions.

Figure 7 shows results of a sensitivity analysis that was carried out on the predicted air exchange at a jet velocity of 18 m.s^{-1}. The purpose of this was to ascertain the accuracy of assumptions made in the model. The 'model used' bar in the figure represents data from the model that is described in this paper (k-ε turbulence model, Bousinnesq approximation, and turbulence intensity (TI) of 10%). The other bars in the figure full buoyancy modelling (not Bousinesq approximation), Reynolds stress turbulence model and TIs of 5 and 20%. The measured bar in the figure shows the infiltration measured in the experiments. All of the assumptions modelled were within 10% of the model used.

Figure 8 shows the predicted air exchange after a door open duration of 10 s for the 'cut down' model at a jet velocity of 18 m.s^{-1}. The predicted air exchange was reducing with finer meshes; however, there was only a 5% reduction in air exchange with the mesh reduced from 100 to 40 mm. The differences due to the assumptions were much lower than the difference between predicted and measured results (47%).
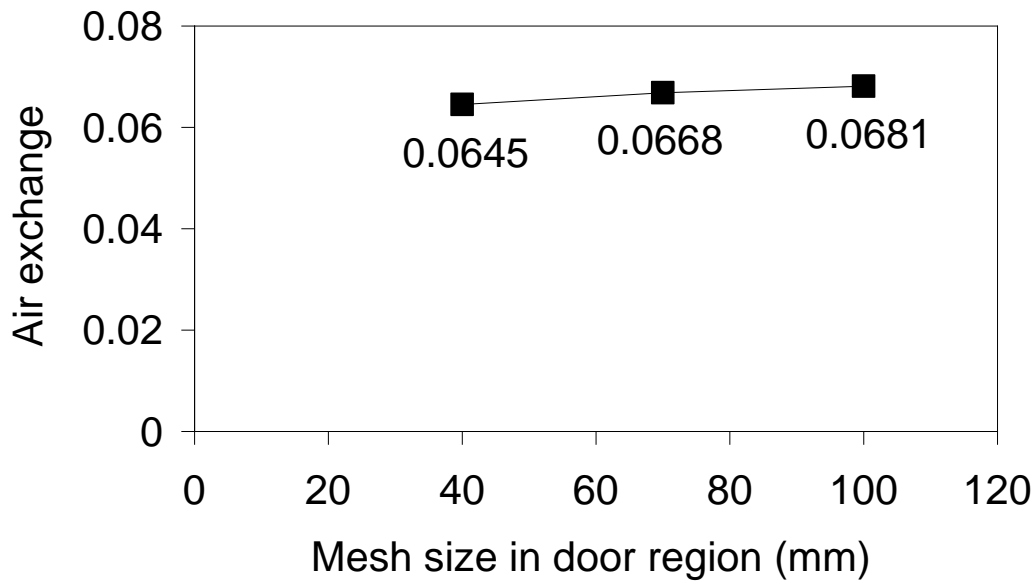
Figure 8. Predicted air exchange at a jet velocity of 18 m.s^{-1} for a door open duration of 10 s for different mesh sizes.

When the door was reduced to 1.0 m wide so that the air curtain fully covered the door with no overlaps, the predicted effectiveness at a jet velocity of 18 m.s^{-1} was 0.59 compared to 0.56 for the 1.36 m door at this velocity, a 5% increase. For the same reduction in door width, the measured effectiveness was increased from 0.71 to 0.79, an 11% increase in the effectiveness.

3.4.1 3-D flow

Figure 9 shows predicted velocity vectors for a vertical elevation in the central plane of the entrance. Although the air curtain leaves the nozzle pointing straight down, the air is very soon deflected away from the room by the Coanda effect, due to the proximity of the fan body. It is not possible to see the 3-D effects of this flow from a single 2-D plane and therefore 3-D iso-velocity plots for 3 different views are shown in Figure 10. The iso-velocity plots show the direction of air flow for all positions at 3 m.s^{-1}. The front elevation shows that the jet narrows in the plane of the entrance. The side

elevation highlights that the centre of the jet is bent out away from the room but the sides are folded back into the room. The plan view shows that the central part of the jet is deflected out of the room (upwards in the figure) and narrows, but that the sides of the jet are drawn into the room and cross one another.
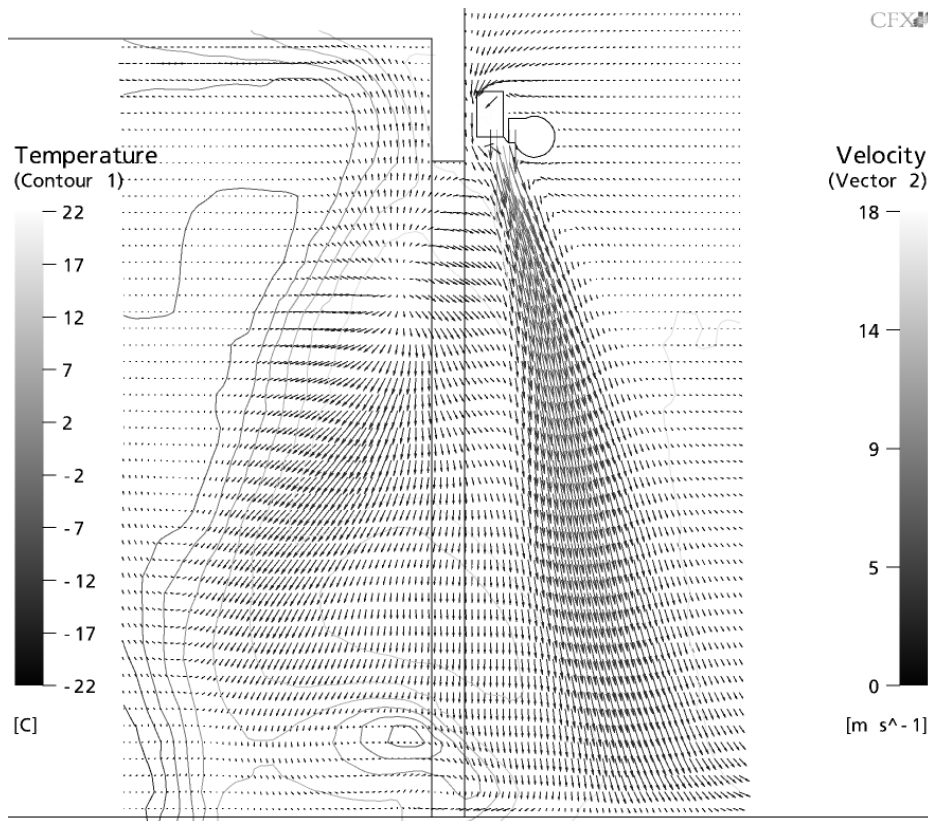

Figure 9. Predicted velocity vectors and temperature contours in the plane of the entrance for a jet velocity of 18 m.s^{-1}, angle of 0[o] and door-open duration of 30 s.

To further understand the effects shown by these predictions further predictions were carried out.

To establish the consequence of the stack effect, the model was repeated isothermally. Results from this showed a similar flow except that the two sides of the jet were deflected towards each other but not into the cold store.

To establish the consequence of the shape of the air curtain body, a simplified, symmetrical air curtain was modelled. The flow was similar to that found when modelling the more realistic air curtain, except that the centre of the jet was not deflected out of the cold store. The sides of the jet were deflected towards each other and into the room but to a much lesser degree.

To establish the consequences of the stack effect on the simplified air curtain, the simplified air curtain was modelled isothermally. The shape of the resulting air curtain was very different to the previously modelled scenarios. The iso-velocity surface was more planar and symmetrical, the jet changing its cross section from a thin rectangle at the nozzle outlet to a broad oval where it strikes the floor. This is much closer to an idealised 2-D air curtain, although 3-D shapes are still present. Due to the lack of stack effect entraining air at the sides of the curtain, the sides of the jet were no longer bent into the cold store and the symmetrical air curtain device meant that there was no unsymmetrical bending of the curtain due to an uneven Coanda effect.

From these models we can deduce that the centre of the jet is deflected away from the cold store because of the proximity and shape of the air curtain body (Coanda effect). The effect of the ends of the jet being bent into the cold store is caused by the stack effect. This is probably because the velocity at the ends of the curtain is reduced, due to entrainment and therefore is less able to resist the stack pressures. In addition gaps at the sides would allow free entry of air and so the shear on the edges of the curtain in an inwards direction towards the top of the curtain would be greater. The effect of the ends of the curtain being deflected towards each other is due to both the stack effect and the shape of the air curtain device. As the centre of the jet is bent away from the cold store, a low-pressure zone is formed, which the jet ends are pulled into.
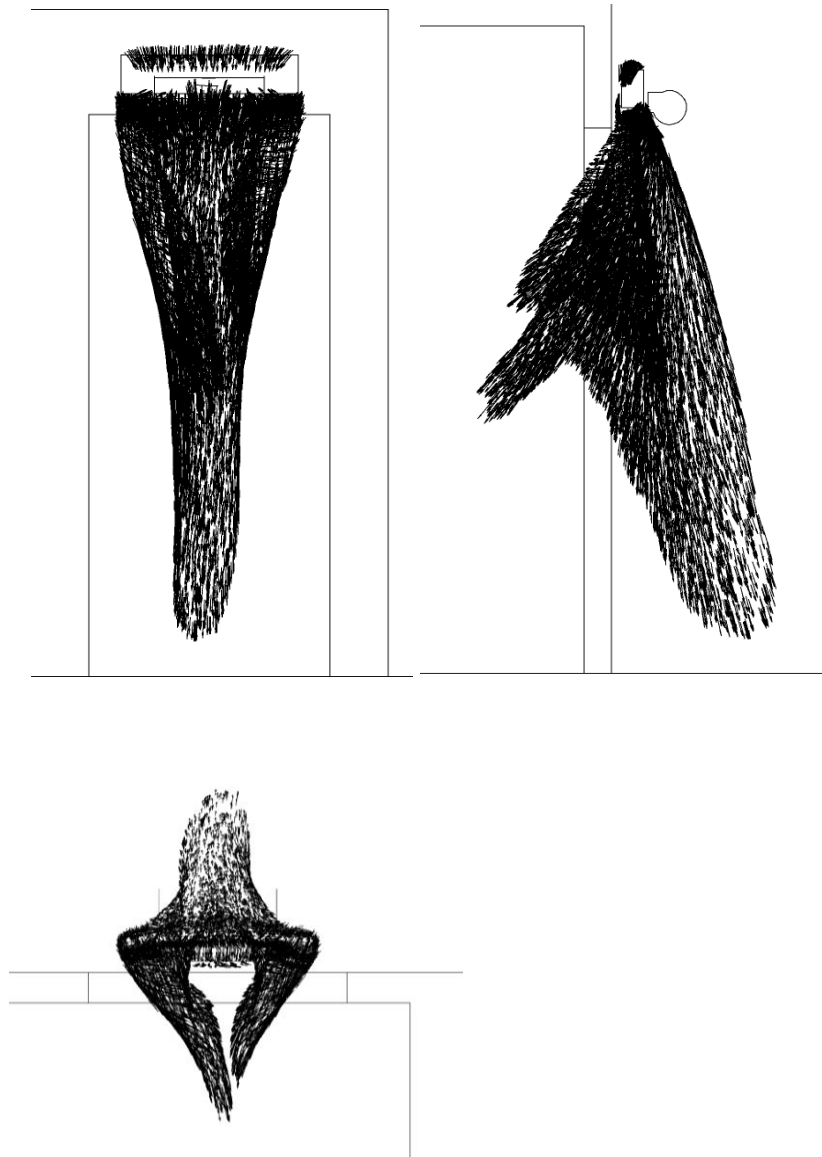
Figure 10. Velocity vectors at a Iso-velocity of 3 m.s^{-1} in the region of the entrance for a jet velocity of 18 m.s^{-1}, angle of 0° and door-open duration of 30 s. Front elevation (left), side elevation (right) and plan view (bottom).

To establish whether an air curtain that covered the full width of the door would have a similar shape, the door was reduced to 1.0 m wide so that the air curtain fully covered the door with no overlaps. The predicted shape of the jet was almost identical to that with the 1.36 m wide door.

4. Conclusions

The effectiveness of an air curtain fitted over a 1.36 m wide entrance to a cold store has been measured and predicted using both 2-D analytical and 3-D CFD models.

This paper has shown the importance of correctly setting up air curtains to give optimal effectiveness. Downing and Meffert [7] reported that air curtains are often not installed at their optimum. This paper has re-enforced those statements using data from controlled experiments.

The analytical model gives a guide to the jet velocity required for an air curtain that seals the entrance as well as possible by reaching the floor. However, these studies have shown that with the air curtain used in these experiments, the effectiveness can vary greatly, depending on which safety factor was chosen in conjunction with the calculated velocities. The analytical model is unable to give any guide on the effectiveness of the air curtain at the different jet velocities, but this work presents the variation in effectiveness with changing safety values.

The 3-D CFD model predicted the infiltration through the entrance with no air curtain to an accuracy of within 20 to 32%. The predicted effectiveness of the air curtain at different jet velocities was 0.08 to 0.15 lower than measured. The trend of the curve of effectiveness against jet velocity was well predicted. Further experimentation with higher jet velocities would have been useful. However, the system was unable to reach velocities that would allow verification of the predicted optimum jet velocity.

Reducing the width of the door to the width of the air curtain had little effect on the predicted shape of the air curtain flow, although it did provide a slight increase in the predicted and measured effectiveness of the air curtain.

It is quite likely that a finer grid mesh would give more accurate predictions, however, the model was fairly accurate at predicting the effectiveness of an air curtain with a coarse mesh (100 mm in the plane of the door) compared to the thickness of the jet (30 mm).

Predictions at different turbulence intensities re-enforced the statement by Guyonnaud et al [18] that they had little effect on air curtain performance.

CFD has shown that the flow from this air curtain cannot be considered as 2-D. The central portion of the air curtain is deflected away from the cold store by the Coanda effect (caused by the fan body). The sides of the curtain are deflected into the cold store by the stack pressures and are drawn into the void caused by the deflected central portion. The same effect is predicted for an air curtain that covers the full width of the door.

Reducing the deflection of the sides of the curtain would probably increase the effectiveness of the air curtain. Either angling the jet outward more at the sides and / or using a higher jet velocity at the sides might do this.

It was not possible to completely validate the effects shown by the CFD work without a tool such as laser Doppler anemometry (LDA) or digital particle image velocimetry (DPIV). However, tufts of tissue paper attached to the air curtain nozzle did show the deflection of the central region of the jet towards the fan body and away from the door entrance.

There were only a finite number of mesh cells available for modelling the experimental set-up, due to memory limitations of the computer. It was not possible, given the size of the domain, to model accurately the exact geometry of the air curtain including the complex return air boundaries. Reducing the domain to just around the air curtain body

would allow a more accurate prediction of the jet exiting the air curtain, however, this would not allow prediction of the effectiveness of the air curtain attached to this cold store. Overcoming this problem would require greater memory than could be achieved using the current 32 bit hardware with a single processor. Running the model on 64-bit hardware or portioning the mesh and solving on a network of computers may overcome this problem.

Acknowledgements

References

[1] Department of Trade and Industry; Estimates derived from UK Office for National Statistics, Future Energy Solutions and Department of Trade and Industry data. http://www.dti.gov.uk/energy/inform/energy_consumption/table4_7.xls; 2002

[2] Boast, M.F.G; Frost free operation of large and high rise cold storage; Proceedings of the Institute of Refrigeration; 2002;6;1-11.

[3] Ligtenburg, P.J.J.H., Wijjfels, D.; Innovative air curtains for frozen food stores. Proceedings of the 19th International Congress of Refrigeration; 1995;420-437.

[4] Hayes, F.C., Stoecker, W.F; Heat transfer characteristics of the air curtain. ASHRAE Transactions; 1969;2120;153-167

[5] Hayes, F.C., Stoecker, W.F; Design data for air curtains. ASHRAE Transactions; 1969;2121;168-180.

[6] Downing, C.C., Meffert, W.A;   Effectiveness of cold-storage door infiltration protective devices (rp-645). ASHRAE Transactions; 1993;99;356.

[7] Emswiler, J.E; The neutral zone in ventilation. Trans. Am. Soc. Heat. Vent. Eng.; 1926;32;1;1-16.

[8] Brown, W.G., Solvason, K.R; Natural convection in openings through partitions-1, vertical partitions. Int. J. Heat Mass Tran.; 1963;5;859-868

[9] Tamm, W; Kälteverluste durch Kühlraumöffnungen. Kältetechnik-Klimatisierung; 1966;18;142-144.

[10] Fritzsche, C., Lilienblum, W; Neue Messungen zur Bestimmung der Kälteverluste an Kühlraumtüren. Kältetechnik-Klimatisierung; 1968;20;279-286.

[11] Gosney, W.B., Olama, H.A.L; Heat and enthalpy gains through cold room doorways. Proceedings of the Instistute of Refrigeration; 1975;72;31-41.

[12] Jones, B.W., Beck, B.T., Steele, J.P; Latent loads in low humidity rooms due to moisture. ASHRAE Transactions; 1983;89;35-55.

[13] Pham, Q.T., Oliver, D.W; Infiltration of air into cold stores. Proceedings of the 16th International Congress of Refrigeration; 1983;4;67-72.

[14] Abramovitch, G.N; The theory of turbulent jets; The M.I.T. press; Cambridge; 1963.

[15] Rajaratnam, N; Turbulent jets; Elsevier Scientific Publishing Company; The Netherlands; 1976

[16] Chen CJ, Rodi, W. Vertical turbulent buoyant jets - a review of experimental data, Permagon Press, Oxford, 1980

[17] Guyonnaud, L. *et al*.; Design of air curtains used for area confinement in tunnel. Exp. Fluids; 2000;28;377-84

[18] Lajos, T., Preszler, L; Untersuchung von Torluftschleieranlagen Teil 1.2. Zeitschrift der Heizung, Lüftung, Klimatechnik, Haustechnik; 1975;26;5;171-176, 6;226-235.

[19] Ge, Y.T., Tassou, S.A; Simulation of the performance of single jet air curtains for vertical refrigerated display cabinets. Appl. Therm. Eng.; 2001;21;2;201-21

[20] Foster, A.M. *et al*; Measurement and prediction of air movement through doorways in refrigerated rooms. Int. J. Refrig.; 2002;25;1102-09

[21] Foster, A.M. *et al*; Experimental verification of analytical and CFD predictions of infiltration through cold store entrances. Int. J. Refrig.; 2003;26;918-25.

[22] Waldron, P; Open door trading. H&V Engineer; 1992;65;713

[23] Longdill, G.R., Frazerhurst, L.F., Wyborn, L.G.; Air curtains - Mirinz 385. In. Hamilton, Meat Research Institute of New Zealand. 1974.

[24] Speziale, C.G., Sarkar, S. and Gatski, T.B; Modelling the pressure-strain correlation of turbulence: an invariant dynamical systems approach" J. Fluid Mech.; 1991;277;245-272

[25] Launder, B.E. and Spalding, D.B; The numerical computation of turbulent flows. Comp. Meth. Appl. Mech. Eng.; 1974;3:269-289

Figure captions

Figure 1. The air curtain device as viewed from below after installation.

Figure 2. Minimum outlet momentum required maintaining an unbroken curtain.

Figure 3: Isometric view of the modelled volumes, illustrating the position of the air curtain and entrance.

Figure 4: Front and side elevations of the modelled air curtain device and air curtain inlet and outlet boundaries.

Figure 5. Geometry of the simplified air curtain used in the CFD model. Front elevation (left) and vertical elevation (right).

Figure 6. Measured and predicted effectiveness of the air curtain for different air jet velocities for a door-open duration of 30s and jet angle of $0°$. The measurements were taken at different outside temperatures (shown in the legend).

Figure 7. Data from a sensitivity analysis showing the predicted air exchange at a jet velocity of 18 $m.s^{-1}$ with different model assumptions.

Figure 8. Predicted velocity vectors and temperature contours in the plane of the entrance for a jet velocity of 18 $m.s^{-1}$, angle of 0° and door-open duration of 30 s.

Figure 9. Velocity vectors at a Iso-velocity of 3 $m.s^{-1}$ in the region of the entrance for a jet velocity of 18 $m.s^{-1}$, angle of 0° and door-open duration of 30 s. Front elevation (left), side elevation (right) and plan view (bottom).